



HAL
open science

Aerodynamic behavior of an airfoil under extreme wind conditions

Ingrid Neunaber, Caroline Braud

► **To cite this version:**

Ingrid Neunaber, Caroline Braud. Aerodynamic behavior of an airfoil under extreme wind conditions. Journal of Physics: Conference Series, 2020, 1618, 10.1088/1742-6596/1618/3/032035 . hal-02888521

HAL Id: hal-02888521

<https://hal.science/hal-02888521>

Submitted on 11 Dec 2020

HAL is a multi-disciplinary open access archive for the deposit and dissemination of scientific research documents, whether they are published or not. The documents may come from teaching and research institutions in France or abroad, or from public or private research centers.

L'archive ouverte pluridisciplinaire **HAL**, est destinée au dépôt et à la diffusion de documents scientifiques de niveau recherche, publiés ou non, émanant des établissements d'enseignement et de recherche français ou étrangers, des laboratoires publics ou privés.

PAPER • OPEN ACCESS

Aerodynamic behavior of an airfoil under extreme wind conditions

To cite this article: Ingrid Neunaber and Caroline Braud 2020 *J. Phys.: Conf. Ser.* **1618** 032035

View the [article online](#) for updates and enhancements.



IOP | ebooks™

Bringing together innovative digital publishing with leading authors from the global scientific community.

Start exploring the collection—download the first chapter of every title for free.

Aerodynamic behavior of an airfoil under extreme wind conditions

Ingrid Neunaber and Caroline Braud

LHEEA (CNRS) - Centrale Nantes, 1 Rue de la Noë, 44300 Nantes, France

E-mail: ingrid.neunaber@ec-nantes.fr

Abstract. Wind turbines operate in the naturally turbulent atmospheric boundary layer. Due to strong flow variations, the aerodynamics at the rotor blades are complex. Therefore, to gain a better understanding of the effect of strong velocity and angle fluctuations on the aerodynamic behavior of an airfoil, we present a new system capable of generating rapid, strong gusts in a wind tunnel, the *chopper*. It consists of a rotating bar cutting through the inlet of the wind tunnel, thus generating turbulent, strong flow perturbations. Using this system and exposing an airfoil to its flow, we investigate the lift variations caused by the simultaneous, rapid velocity and angle variations. The results show that the lift response of the airfoil is directly correlated with the velocity. The lift response to changes of the angle of attack is determined not only by the change of the angle, but also by the rapidity with which it changes.

1. Introduction

Wind energy converters operate in the turbulent atmospheric boundary layer. The atmospheric turbulence is highly complex with three-dimensional, multi-scale vortices of varying frequencies. Therefore, the rotor of a wind energy converter faces various inflow situations in very short times. These turbulent inflow variations change the aerodynamic behavior on the rotor blades which increases fatigue loads and failure rates (see e.g. [4],[9]). One particular example of inflow variations are extreme wind conditions. In order to guarantee a wind turbine's safety and durability within its 20 year lifespan, the IEC-61400-1 standard includes these extreme operating conditions in form of artificial wind gusts [8].

The interaction between complex, rapid flow structures and the rotor blade is not well understood, as the aerodynamic behavior of an airfoil is highly dependent on the dynamic variations of the angle of attack between the flow and the blade. For example, dynamic stall can occur which causes rapid changes in the lift and thus induces high loads, see e.g. [5], [11]. One possibility to improve the comprehension of the aerodynamic effects acting on the blade due to complex flow is by means of wind tunnel investigations with a two-dimensional airfoil. One device capable of generating the complex, gusty flows needed for these investigations is a Makita-style active grid. Grids of this type have been used in the past for example to generate the artificial gust proposed in the IEC-61400-1 standard, see e.g. [10]; [13], [15], [18]. Often, however, the inflow is simplified so that only the influence of isolated aspects of the inflow variations are scrutinized. This is for example done by generating clean, sinusoidal inflow variations by using slotted, rotating cylinders, [14], or by using a pitching and plunging airfoil, [17], or oscillating plates in the inlet of the wind tunnel, [16]. Also, when prioritizing the variation of the mean



flow, the "background" turbulence is often neglected in experimental research although the atmospheric wind is turbulent *with* gusts.

Therefore, in this study, we present a new setup that is capable of generating reproducible, rapid, strong velocity and flow angle variations in a wind tunnel while simultaneously including turbulent fluctuations. After the experimental setup is explained, first, the flow generated by this new system will be presented, and afterwards, the lift response of an airfoil is investigated with respect to the flow variations.

2. Setup

In the following, the setup used in this study is presented. A sketch can be found in figure 1. The measurements are carried out in a wind tunnel with an inlet of $0.5 \text{ m} \times 0.5 \text{ m}$ and a closed test section of 2.3 m length. The background turbulence intensity of the empty wind tunnel is $TI = 0.3\%$, and a regular grid with 16.4% blockage and a mesh width of 7 cm is installed inside the nozzle which increases the background turbulence intensity to $TI \approx 3.0\%$. This was done to improve the aerodynamic response of the airfoil at low Reynolds numbers (see e.g. [3]).

To generate complex three-dimensional flow structures, a new perturbation system was installed. It is called the *chopper*, and it consists of a rotating bar, the *chopper blade*, that is passing through the inlet of the test section as illustrated in figure 1. This creates a perturbation in form of a turbulent inverse gust due to the blockage (cf. [12], see figure 2 and section 3.1). The chopper blade has a radius of 90 cm , a width of 10 cm , and a thickness of 5 cm . As demonstrated in [12] with a chopper blade of 20 cm width, the inverse gust can be modified by means of the blade passing frequency of the chopper blade, the *chopper frequency* f_{CH}^1 , that is measured with an induction sensor. In addition, the downstream position can be used to alter the inflow condition as the gust disperses downstream.

In this study, an airfoil with a chord length of $c = 9 \text{ cm}$ is mounted 158.5 cm downstream of the inlet where the average flow field generated by the chopper is homogeneous. A force gauge measures the lift force F_L acting on the airfoil. Prior to the experiments, the lift coefficient

$$c_L = \frac{F_L}{0.5 \cdot \rho \cdot A \cdot u_0^2} \quad (1)$$

was determined for different chord-based Reynolds numbers $Re = \frac{c \cdot u_0}{\nu}$ (cf. figure 1) in the turbulent inflow generated by the regular grid (the chopper is not running). Here, ρ denotes the air density, ν is the kinematic viscosity, $A = 9 \text{ cm} \cdot 50 \text{ cm}$ is the airfoil's surface, and u_0 is the inflow velocity. The inflow velocity ranges from $u_0 = 12 \text{ ms}^{-1}$ to $u_0 = 20 \text{ ms}^{-1}$. At low angles of attack $0^\circ \leq \alpha \leq 6^\circ$ and low velocities (lower than $u_0 = 17 \text{ ms}^{-1}$), low Reynolds number effects cause a dependence of c_L on the inflow velocity. Currently, we are restricted to rather low Reynolds numbers due to the limited measurement range of the force gauge but we will change this in future experiments.

Simultaneously, the three components of the inflow velocity are measured with one cobra probe in front of the airfoil, and the sampling frequency is $f_s = 2.5 \text{ kHz}$. In addition, a 1D hot-wire was used to measure the high-frequent flow variations at the same position with a sampling frequency of $f_s = 50 \text{ kHz}$, and a hardware low-pass filter with a cut-off frequency of 20 kHz was used.

The measurements with the chopper have been carried out at two different chopper frequencies, $f_{CH1} = 0.04 \text{ Hz}$ and $f_{CH2} = 0.4 \text{ Hz}$, one inflow velocity ($u_0 = 18 \text{ ms}^{-1}$), and three different set airfoil angles α_0 , $\alpha_{01} = -0.02^\circ$, $\alpha_{02} = 7.8^\circ$, and $\alpha_{03} = 12.11^\circ$. The α_0 were chosen to cover the range where c_L depends on the Reynolds number. The two exemplary chopper frequencies were chosen so that the generated gusts would

¹ Note that by this definition, the chopper frequency is twice the rotational frequency of the chopper blade.

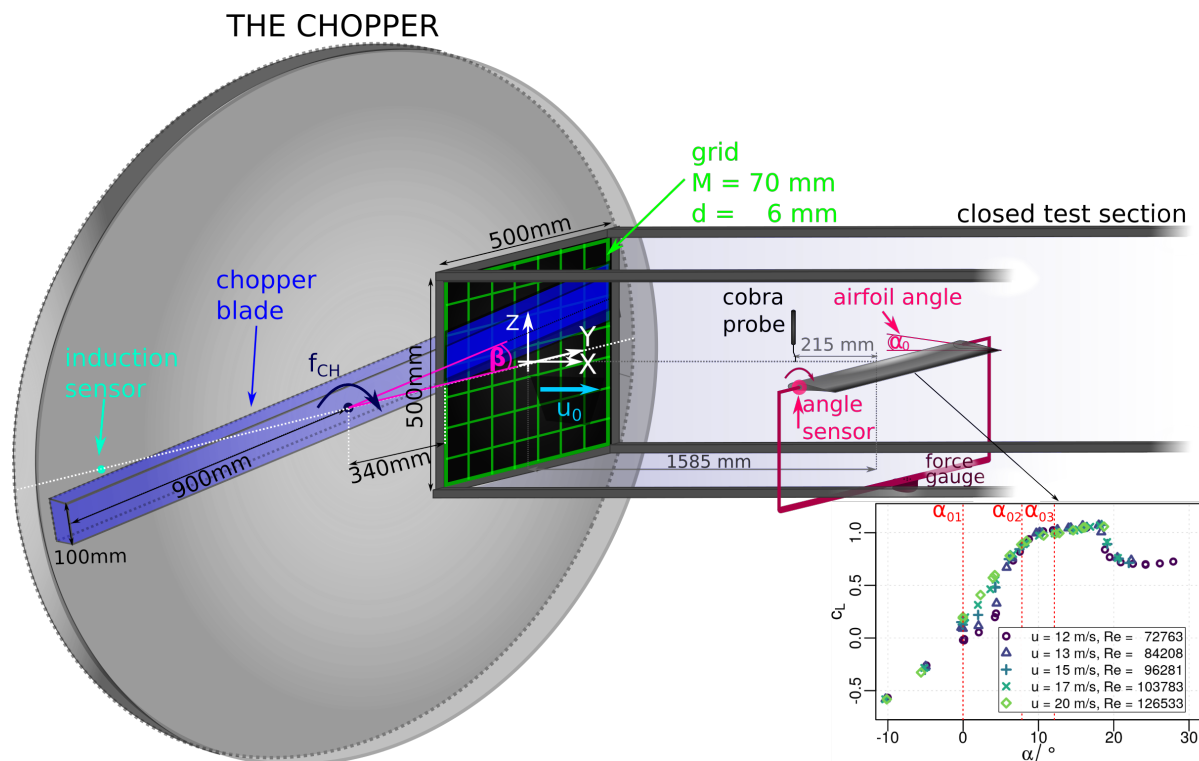


Figure 1. Experimental setup: The chopper blade passes through the inlet of the wind tunnel, thus generating a flow perturbation that is measured with a cobra probe (or 1D hot-wire) in front of the airfoil. This inverse gust passes the airfoil that is mounted downstream in the test section on a force gauge. The angle of attack is measured with an angle sensor. In addition, the lift coefficient c_L is plotted over α for different Re , and the airfoil angles α_0 used in the experiment are indicated.

- have a characteristic time Δt similar to the artificial gust proposed in the IEC standard $\Delta t_{IEC} = 10.5$ s
- have a characteristic time that is scaled down to wind tunnel dimensions by keeping the ratio between the characteristic time and the chord length $\Delta t/c$ constant. As compared to full scale measurements with $\Delta t/c \approx 10$ s/1 m, this yields $\Delta t/c \approx 0.9$ s/0.09 m for the experiment we want to carry out.

The inflow velocity was chosen above the velocity range in which low Reynolds number effects are present (see lift curve in figure 1). The measurement times were adapted to the chopper frequency, $t_{M1} = 600$ s for f_{CH1} and $t_{M2} = 120$ s for f_{CH1} . The acquisition time was chosen to be sufficiently long to reach a statistical convergence of the phase average of the inverse gust events. This is demonstrated by figure 2 where the evolution of the phase average over an increasing number of gusts towards a mean gust shape is plotted. The single gust events were extracted from one time series obtained from hot-wire measurements. From this plot, it becomes obvious that the flow of a single gust is highly turbulent due to the shear that is induced by the chopper blade. Also, the turbulence generated by the grid is visible outside of the actual gust event. Despite the strong turbulence, already a comparatively small number of gusts suffices to reach the statistical convergence.

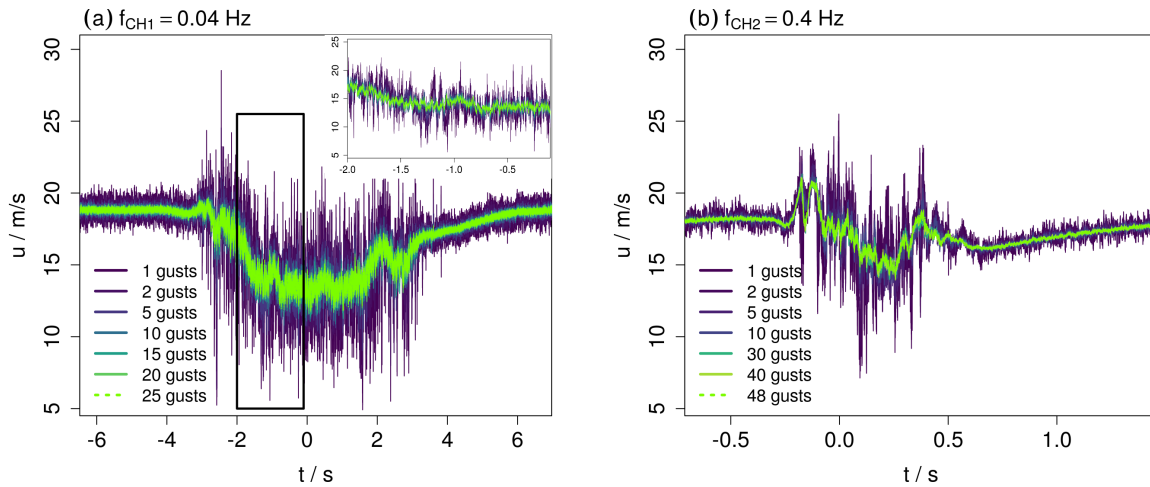


Figure 2. Example of one gust event (dark purple) in addition to phase averages over an increasing number of gust events to visualize the statistical convergence. The measurements were performed with a 1D hot-wire for the two chopper frequencies $f_{CH1} = 0.04$ Hz, (a), and $f_{CH2} = 0.4$ Hz, (b).

3. Results

In the following, the results of this study will be presented. First, the inflow characteristics will be briefly discussed, and afterwards, the airfoil's response to the inverse gust is examined.

3.1. Inflow conditions

For a first idea of the inflow generated by the chopper, it is useful to look at a part of the time series of the stream-wise velocity measured with a 1D hot-wire. This is done in figure 3 for both chopper frequencies. In addition, the blockage induced by the chopper blade is indicated. It can be seen that the recurring inverse gust events can be separated from the periods where the chopper blade does not block any part of the wind tunnel. In [12], it was shown that the inverse gust can be separated into a mean velocity, an underlying gust shape and the turbulence within the gust. For both chopper frequencies, the inverse gusts show stronger fluctuations than the background flow. When the chopper blade enters the wind tunnel, the velocity first briefly increases before the velocity drops in the wake of the chopper blade. Before discussing the velocity evolution more detailedly, we will first investigate the energy spectral density.

In figure 4, the energy spectral density $E(f)$ of the time series shown in figure 3 is plotted over the frequency f for both chopper frequencies. The periodic gust event is indicated by the peak in the spectrum and its harmonics. As was shown in [12], the high-frequency part of the spectrum that decays according to $E \propto f^{-5/3}$ is due to the turbulence in the gust². As the grid had not been installed during the experiments presented in [12], we can conclude that the effect of the background turbulence generated by the regular grid on the decay region of the energy spectrum is negligible.

To further discuss the inflow conditions, a detailed view on the inverse gust shape is given. For this, the phase-averaged, smoothed inverse gust is presented in figure 5 for both chopper frequencies. The smoothing was performed using a moving average with the window size adapted proportionally to the chopper frequency, $\tau(f_{CH1}) = 0.2s$ and $\tau(f_{CH2}) = 0.02s$. The measurements were obtained using the cobra probe, and all three velocity components are shown.

² Note, that this decay is not related to the scaling of the spectrum with dissipation in equilibrium as proposed by [6] and [7]. For a detailed explanation, see [12].

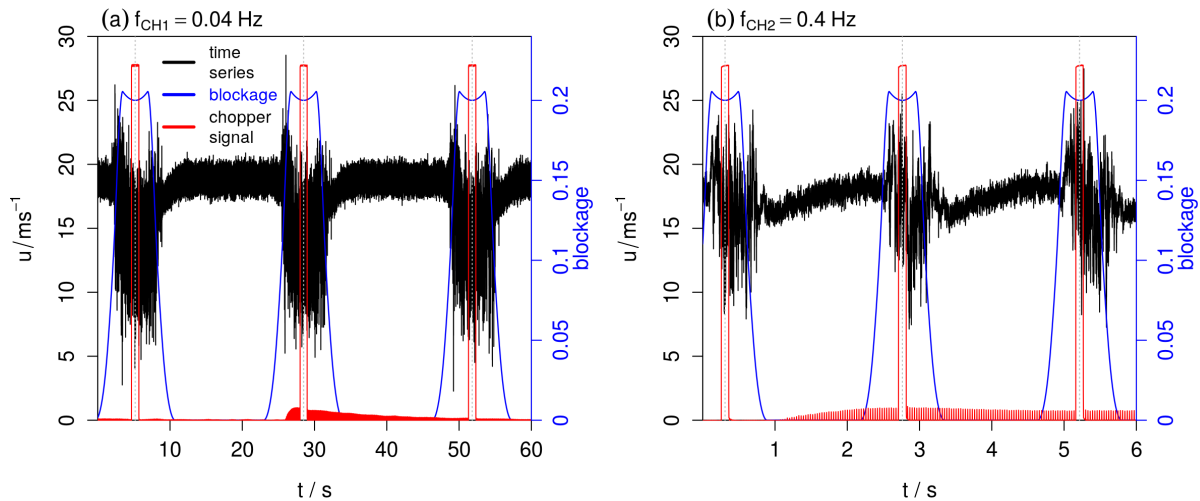


Figure 3. A part of the time series that shows three gusts is plotted for the two chopper frequencies $f_{CH1} = 0.04$ Hz, (a), and $f_{CH2} = 0.4$ Hz, (b). The measurements were carried out using a 1D hot-wire. In addition, the signal of the induction sensor is plotted in red (arbitrary units) and the blockage is plotted in blue with the corresponding blue axis at the right side of the plot.

In addition, the blockage induced by the chopper blade is indicated.

In the case of f_{CH1} , the absolute velocity U of the inverse gust decreases by approximately 5 ms^{-1} within approximately 1.6 s from the inflow velocity $u_0 \approx 18 \text{ ms}^{-1}$ to $U \approx 13 \text{ ms}^{-1}$. The velocity remains low while the blockage induced by the chopper blade is maximal. As the velocity correlates with the blockage, it recovers when the chopper blade leaves the wind tunnel. The velocity recovery time, 3.2 s, is slower than the velocity decrease time. The span-wise v component is 0 between the gusts and varies around $v = 0 \text{ ms}^{-1}$ when the chopper blade enters. The maximal amplitude is $\Delta v \approx 1.3 \text{ ms}^{-1}$. The wall-normal w component is also 0 in the free flow. It increases to $w \approx 0.7 \text{ ms}^{-1}$ when the chopper blade enters, then decreases to $w \approx -1.0 \text{ ms}^{-1}$ and tends to 0 again when the chopper blade is leaving the wind tunnel. By means of the time period where the w flow component is different from 0, a gust characteristic time $\Delta t \approx 7.5 \text{ s}$ was determined. Note that the time during which the absolute and stream-wise velocities vary from the inflow velocity u_0 is longer. The mean gust properties are summarized in table 1.

In case of f_{CH2} , the inverse gust shows more dynamic. U first shows a short, fast velocity increase of more than 2.3 ms^{-1} in 0.05 s. After a drop and a second increase, the velocity drops by 4.25 ms^{-1} in 0.06 s. Next, the velocity decreases more slowly but then increases again rapidly by approximately 4 ms^{-1} in 0.14 s. The amplitude of the absolute gust velocity is more than 6 ms^{-1} . The increase of the absolute velocity in the beginning is accompanied by an increase of the w flow component. Afterwards, the w flow component varies and is mostly negative, and the v component also does not show any strong fluctuations. By means of the w flow component, a gust characteristic time $\Delta t \approx 0.8 \text{ s}$ was determined, which indicates that the gust characteristic time is roughly anti-proportional to the chopper frequency. A summary of all gust properties can be found in table 1.

Although the gusts look at first glance quite different apart from the induced velocity deficit, it could be shown in [12] that distinctive features like the small velocity increase in the beginning of the gust can be explained physically. For a detailed explanation of the inverse gust and the physical effects that lead to it, the reader is referred to [12].

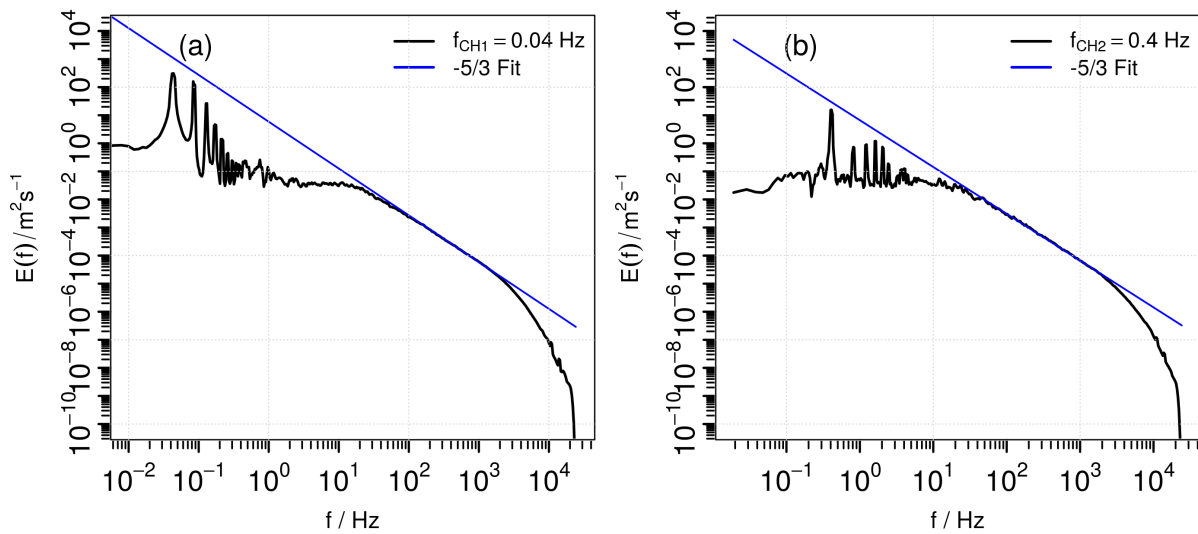


Figure 4. Energy spectral density of the stream-wise velocity component measured with a 1D hot-wire 21.5 cm in front of the airfoil ($\alpha_{02} = 7.8^\circ$) for the two chopper frequencies $f_{CH1} = 0.04$ Hz, (a), and $f_{CH2} = 0.4$ Hz, (b).

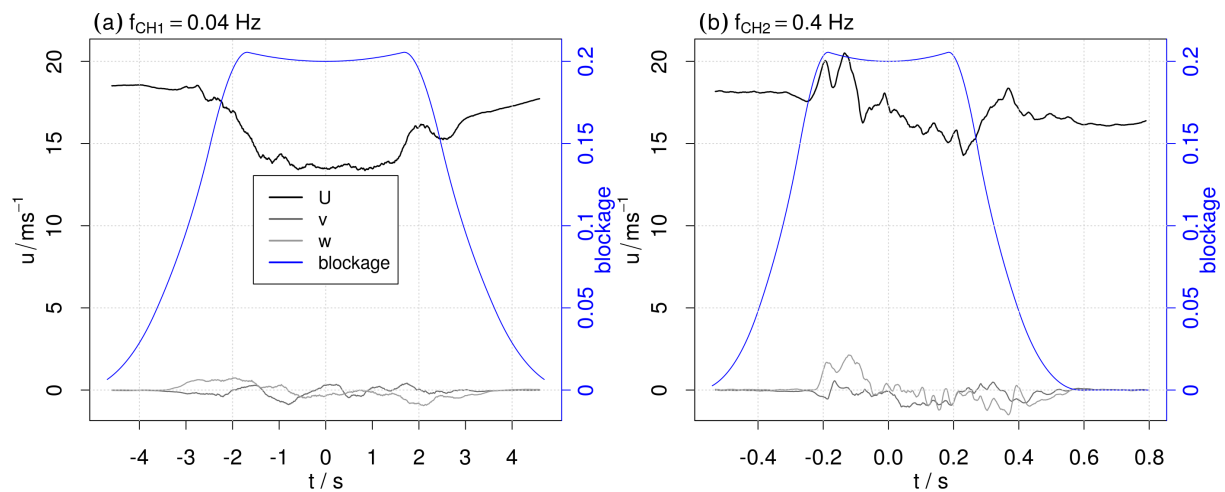


Figure 5. Smoothed velocity components U (black), v (dark gray) and w (light gray) for $u_0 = 18 \text{ ms}^{-1}$ and the two chopper frequencies $f_{CH1} = 0.04$ Hz, (a), and $f_{CH2} = 0.4$ Hz, (b). In addition, the blockage induced by the chopper is plotted in blue.

To briefly comment on the comparability of this artificial gust, the extreme operating gust of the IEC-61400-1 standard, and gusts in the atmospheric flow, we will compare the commonly used gust factor

$$G_I = \frac{U_{max}}{\bar{U}_I} \quad (2)$$

where U_{max} denotes the maximum wind speed in a time interval I and \bar{U}_I denotes the mean wind speed in this interval [1]. In our case and the IEC extreme wind case, the interval equals the gust characteristic time. Thus, the calculated gust factors are $G_I(f_{CH1}) = 1.16$ and $G_I(f_{CH2}) = 1.2$.

For an exemplary extreme operating gust calculated according to the IEC 61400-1 standard³, $G_{I,IEC} = 1.27$ at $u_0 = 20 \text{ ms}^{-1}$. As shown in [1], these are typical values also for field measurements.

3.2. Airfoil response

In the following, the lift force acting on the airfoil as a response to the inverse gust will be investigated. For this, figure 6 shows the phase-averaged, smoothed lift force response for the respective chopper frequency and the three angles of attack. In addition, the plots show the phase-averaged, smoothed inverse gust and the respective gust-induced flow pitch angle ψ . ψ is plotted instead of the w flow component to directly see the variation in the angle of attack $\alpha = \alpha_0 + \psi$ between the airfoil with the set airfoil angle α_0 and the gust-induced flow pitch angle. For both chopper frequencies, the lift response follows the respective shape of the inverse gust's velocity. The higher the angle of attack, the higher the lift force acting on the blade. In the case of f_{CH2} , it can be seen that the inverse gust is captured first by the cobra probe (black vertical line as exemplary indication in figure 6 (b)) and then by the airfoil (red vertical line in figure 6 (a)). This time delay, $\delta t \approx 0.02 \text{ s}$, is related to the gust's convection velocity $U = 17 \text{ ms}^{-1}$, as the length $\delta x \approx 34 \text{ cm}$ that corresponds to δt is close to the distance between the cobra probe and the airfoil's leading edge, 21.5 cm. The evolution of the lift response appears to be independent of the gust-induced flow pitch angle in the case of f_{CH1} . However, in the case of f_{CH2} , the gust-induced flow pitch angle evolves similarly to the stream-wise velocity and therefore similarly to the lift response.

To quantify the lift response, table 2 summarizes the maximum lift force $F_{L,max}$, the minimum lift force $F_{L,min}$, and the lift force amplitude ΔF_L for the three angles of attack and the two chopper frequencies. In the case of f_{CH1} , the velocity amplitudes are lower as compared to those in the case of f_{CH2} , and the same applies to the lift force amplitudes. While at $\alpha = -0.02^\circ$ and f_{CH1} , the lift force amplitude is significantly lower than for the other angles of attack, ΔF_L is similar in case of f_{CH2} for all angles of attack. The highest lift force amplitudes are found for $\alpha = 7.8^\circ$. This suggests that not only the gust velocity influences the lift response. This is also supported by a repetition of this experiment at a higher inflow velocity and thus Reynolds number of 20.5 ms^{-1} , that is not presented here but that has the same results.

Another indication of a dynamic response of the airfoil is the reduced frequency (cf. e.g. [2])

$$k = \frac{\pi \cdot f_f \cdot c}{u_0} \quad (3)$$

where f_f denotes the frequency of the flow variation. When using the chopper frequency as variation period, this yields $k_1(f_{CH1}) = 0.0006$ and $k_2(f_{CH2}) = 0.006$. From [2], we know

³ A wind turbine of class *I.A* with a diameter of 136 m and a hub height of 155 m was assumed.

Table 1. Summary of gust properties for both chopper frequencies. The velocity components are in ms^{-1} .

	$\Delta t/\text{s}$	U			v			w		
		U_{max}	U_{min}	ΔU	v_{max}	v_{min}	Δv	w_{max}	w_{min}	Δw
f_{CH1}	7.3	18.6	13.4	5.2	0.4	-0.9	1.3	0.7	-0.9	1.6
f_{CH2}	0.8	20.5	14.3	6.2	0.6	-1.0	1.6	2.1	-1.5	3.6

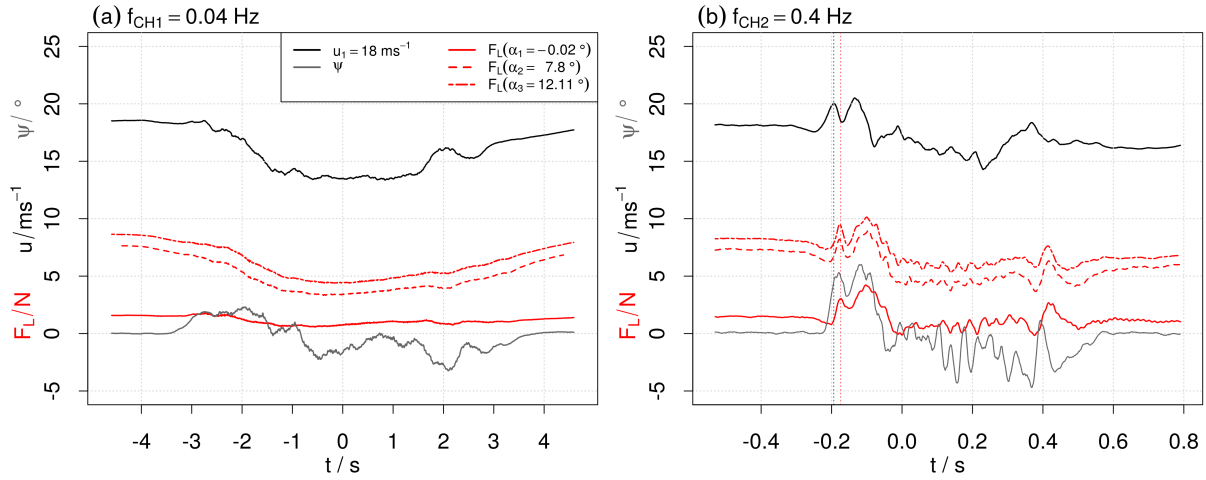


Figure 6. Airfoil's lift response to the gust: The gust velocity (black), the gust-induced flow pitch angle ψ (gray) and the lift force response for the three airfoil angles -0.02° , 7.8° and 12.11° (red, different line types) are plotted for $f_{CH1} = 0.04$ Hz, (a), and $f_{CH2} = 0.4$ Hz, (b).

that dynamic effects can be present already at $k = 0.01$ and thus, an influence might be expected for f_{CH2} . Since we are not investigating a typical periodic flow, it might be worth looking at $k^* = \frac{\pi \cdot c}{\Delta t \cdot u_0}$ that takes into consideration the gust characteristic time. Here, we have $k_1^*(f_{CH1}) = 0.002$ and $k_2^*(f_{CH2}) = 0.02$ which indicates that dynamic effects are even more likely to occur.

To further investigate this result, we use an interpolated surface fit of the $c_L(\alpha, u_0)$ curves to determine the response of the lift coefficient to the gust that would be expected for a respective angle of attack α and velocity U , and we compare the results to the measured response of the lift coefficient for both chopper frequencies at $\alpha_{02} = 7.8^\circ$. The results are presented in figure 7. To distinguish between the influence of the velocity and the gust-induced flow pitch angle, the simulated lift coefficient is calculated with respect to both U and ψ , with respect to U when the nominal airfoil angle α_0 is assumed, and with respect to ψ when the average velocity of the inverse gust is used. It can be seen that for both chopper frequencies, the simulated lift coefficient response is determined by the change of the angle of attack $\alpha = \alpha_0 + \psi$. With respect to the gust velocity, the response of c_L would be constant. Compared to the measured response of c_L , the results are in the case of f_{CH1} in the same order of magnitude. However, the measured evolution does not match the simulated evolution which could be interpreted as additional aerodynamic

Table 2. Lift force response of the airfoil at the three angles of attack to the inverse gust for both chopper frequencies: maximum lift force $F_{L,max}$, minimum lift force $F_{L,min}$ and lift force amplitude ΔF_L in N.

	$\Delta U/\text{ms}^{-1}$	$\alpha_{01} = -0.02^\circ$			$\alpha_{02} = 7.8^\circ$			$\alpha_{03} = 12.11^\circ$		
		$F_{L,max}$	$F_{L,min}$	ΔF_L	$F_{L,max}$	$F_{L,min}$	ΔF_L	$F_{L,max}$	$F_{L,min}$	ΔF_L
f_{CH1}	5.2	1.79	0.56	1.23	7.65	3.32	4.33	8.65	4.39	4.26
f_{CH2}	6.2	4.22	-0.16	4.38	8.99	3.67	5.32	10.14	5.31	4.83

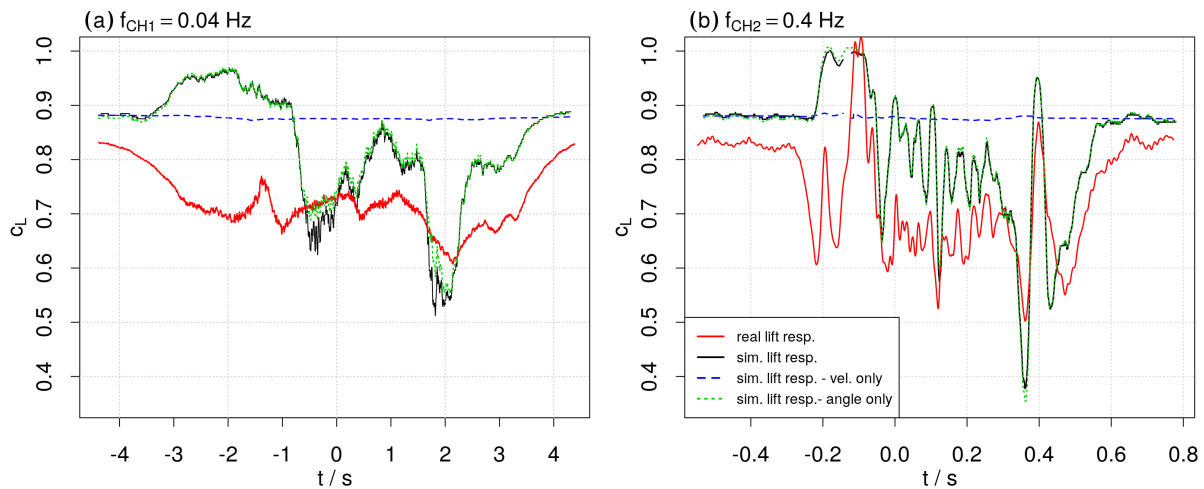


Figure 7. Simulated and calculated lift coefficient c_L at $\alpha_{02} = 7.8^\circ$ for $f_{CH1} = 0.4$ Hz, (a), and $f_{CH2} = 0.04$ Hz, (b), respectively: c_L is simulated with respect to the gust velocity and gust-induced flow pitch angle (black), the gust-induced flow pitch angle only (green, dot-dashed), and the velocity only (blue, dashed).

effects being involved, possibly by moving to the Reynolds number sensitive region of the lift curve in the dynamic flow. In contrast, the simulated and measured c_L response match quite well in the case of f_{CH2} . This means that here, the changing angle of attack α mainly determines the lift response. With respect to the reduced frequency, these results are particularly interesting because in contrast to other experiments, here, the aerodynamic behavior is not bound to an increase of k .

The offset between simulated and measured c_L is assumed to be related to different methods of measuring the inflow velocity since the velocity measured by the cobra probe will already be influenced by the presence of the airfoil. This will be optimized in future measurements.

For the other two airfoil angles that were investigated, we observe similarly that the difference between the simulated c_L and the measured c_L is larger for the slow chopper frequency f_{CH1} than for f_{CH2} .

Further investigations of the aerodynamic effects are necessary but out of the scope of this study.

4. Discussion and Conclusions

In this paper, we present a device that induces complex flow situations for aerodynamic experiments. It is called the *chopper*, and we showed an analysis of the inflow together with the first measurements of the aerodynamic lift force acting on an airfoil in this flow. First, the inflow generated by the chopper was examined carefully by means of the time series, the energy spectral density and the three flow components of the phase-averaged, smoothed gust shape for the two different chopper frequencies. By means of the time series and the energy spectral density, the time series can be separated into the periodically recurring gust event (indicated by the peaks in the spectrum corresponding to the chopper frequency) and the turbulence within the gust. It was shown that in the absolute velocity, an inverse gust is generated that follows the blockage in the case of f_{CH1} but is more complex with larger flow variations in the case of f_{CH2} . While the span-wise velocity component v has a small amplitude during the gust, higher variations are found in the wall-normal velocity component w and consequently in the gust-induced flow pitch angle. The gust characteristic time, here defined as the time during which the wall-normal flow

component varies, scales roughly anti-proportionally with the chopper frequency.

Next, the response of the lift force acting on an airfoil at three different airfoil angles was examined for the two chopper frequencies. It was confirmed that the lift force increases with increasing angle of attack. The lift force response matches the absolute gust velocity for the respective chopper frequencies. This has also been confirmed for a higher inflow velocity in measurements that are not presented in this paper. Therefore, the influence of the inflow velocity plays a secondary role despite the sensitivity of the c_L response to the velocity for low angles of attack. A comparison of the simulated and measured lift coefficients reveals that for f_{CH2} , i.e. for an inflow situation with rapidly changing stream-wise velocity and gust-induced flow pitch angle, the determining quantity is the gust-induced flow pitch angle. However, in the case of f_{CH1} where the variations are slow, different aerodynamic effects, possibly related to the low Reynolds numbers in this study, influence the lift force response of the airfoil. When looking at the reduced frequency k , this result is interesting as aerodynamic anomalies would be expected at higher chopper frequencies.

This study presents a first investigation of the global aerodynamic response of an airfoil exposed to the flow generated by a new gust generating system. An important result is that in highly dynamic, gusty flows, the airfoil's lift response can not be determined from the static lift response, a method, that is normally used in e.g. Blade Elementum Method codes. The next step will be to investigate the local aerodynamic behavior by combining non-intrusive flow measurements (e.g. Particle Image Velocimetry) with local aerodynamic characterization (e.g. unsteady wall pressure measurements).

Acknowledgements

This work was carried out within the research projects ASAPe with the funding from region Pays-de-Loire, Centrale Nantes, and Ville de Nantes (grant no. 2018 ASAPe) and ePARADISE with the funding from ADEME/region Pays-de-Loire (grant no. 1905C0030). The authors would like to thank the West Atlantic Marine Energy Community (WEAMEC). The authors would also like to thank the Scientific and Technical Center for Building (CSTB) for providing measurement equipment.

References

- [1] Bardal L M and Sætran L R 2016 Wind gust factors in a coastal wind climate *Energy Procedia* **94**, 417–424
- [2] Choudhry A, Leknys R, Arjomandi M and Kelso R 2014 An insight into the dynamic stall lift characteristics *Experimental Thermal and Fluid Science* **58**, 188208
- [3] Devinant Ph, Laverne T, and Hureau J 2002 Experimental study of wind-turbine airfoil aerodynamics in high turbulence *Journal of Wind Engineering* **90**, 689–707
- [4] Frandsen S 2007 Turbulence and turbulence generated structural loading in wind turbine clusters, Phd thesis DTU - Risø National Laboratory
- [5] Granlund K, Monnier B, Ol M, and Williams D 2014 Airfoil longitudinal gust response in separated vs. attached flows, *Physics of fluids* **58** 188–208
- [6] Kolmogorov A N 1941a The Local Structure of Turbulence in Incompressible Viscous Fluid for Very Large Reynolds Numbers, *Akademiia Nauk SSSR Doklady* **30**
- [7] Kolmogorov A N 1941b Dissipation of energy in locally isotropic turbulence, *Akademiia Nauk SSSR Doklady* **32**
- [8] IEC 61400-1-4 2019 Wind energy generation systems - Part 1: Design requirements, Report, *International Electrotechnical Commission*
- [9] Lee S, Churchfield M, Moriarty P, Jonkman J, and Michalakes J 2012 Turbulence Impacts on Wind Turbine Fatigue Loadings, *50th AIAA Aerospace Sciences Meeting including the New Horizons Forum and Aerospace Exposition, Aerospace Sciences Meetings* pp. 175–191
- [10] Makita H 1991 Realization of a large-scale turbulence field in a small wind tunnel, *Fluid Dynamics Research* **8**, 53-64
- [11] Mulleners K, and Raffel M 2012 The onset of dynamic stall revisited *Exp. Fluids* **52**, 779793

- [12] Neunaber I, and Braud C 2020 First characterization of a new perturbation system for gust generation: The Chopper *Wind Energy Science* **5**, 759–773
- [13] Petrović V, Berger F, Neuhaus L, Hölling M, and Kühn M 2019 Wind tunnel setup for experimental validation of wind turbine control concepts under tailor-made reproducible wind conditions, *J. Phys.: Conf. Ser.*, **1222**, 012013
- [14] Tang D M, Paul G A, and Dowell E H 1996 Experiments and Analysis for a Gust Generator in a Wind Tunnel, *J Aircraft* **33**, 1
- [15] Traphan D, Wester T T B, Peinke J, and Gülker G 2018 On the aerodynamic behavior of an airfoil under tailored turbulent inflow conditions, *Proceedings of the 5th International Conference on Experimental Fluid Mechanics ICEFM 2018 Munich*
- [16] Wei N J, Kissing J, Wester T T B, Wegt S, Schiffmann K, Jakirlic S, Hlling M, Peinke J, and Tropea C 2019a Insights into the periodic gust response of airfoils, *Journal of Fluid Mechanics* **876**, 237263
- [17] Wei N J, Kissing J, and Tropea C. 2019b Generation of periodic gusts with a pitching and plunging airfoil, *Experiments in Fluids* **60** 166
- [18] Wester T T B, Kampers G, Gülker G, Peinke J, Cordes U, Tropea C, and Hölling M 2018 High speed PIV measurements of an adaptive camber airfoil under highly gusty inflow conditions, *J. Phys.: Conf. Ser.* **1037** 072007